International Journal of GEOMATE, March., 2023, Vol.24, Issue 103, pp.128-135
ISSN: 2186-2982 (P), 2186-2990 (O), Japan, DOI: https://doi.org/10.21660/2023.103.3765
Geotechnique, Construction Materials and Environment

DYNAMIC EFFECTS OF THE HEAD EDGE BEHAVIOR OF GRAVITY CURRENT

*Jinichi Koue[1]

[1] Graduate school of Maritime Sciences, Kobe University, Japan;

*Corresponding Author, Received: 30 Dec. 2022, Revised: 28 Jan. 2022, Accepted: 14 Feb. 2023

ABSTRACT: The flow of the gravity current plays an important role in the transportation and mixing of dissolved or suspended nutrients and chemical substances. In this study, from the experiments and numerical simulations of locked-exchange flow, the flow structure at the head of the gravity current was investigated. In a rectangular channel, a finite volume of fluid was instantaneously released into another fluid of slightly different density. A comparison of theoretical methods, experiments and numerical simulations showed that the water depth and volume of the released fluid affected the velocity of the gravity current. In the initial stage, the head moved forward at a constant velocity and then decelerated. In the final stage, which was governed by viscosity, the front velocity decreased proportionally to the time to the power of 1/2 when the head was not disturbed from behind. Gravity current created a mass concentration at the head in the initial stage. As the mass concentration at the head decreased, the gravity current was slowed down by the viscous stage due to the effect of the bottom friction according to the theoretical analysis. In the viscous stage, the mass concentration at the head no longer existed. The transition stage from the initial stage to the viscous stage was shown to vary with the Reynolds number by the numerical simulation. Clarification of the behavior of the leading edge of gravity flow will help predict the formation of mass transport in oceans and lakes, contributing to the conservation of the aquatic environment.

Keywords: Gravity current; Head edge; Transition; Transport processes

1. INTRODUCTION

Gravity currents, also known as density currents, are primarily driven by the density difference between two fluids moving horizontally. They are generated naturally by currents, coastal upwelling, and mud flow at the sea's bottom, but they can also be caused artificially by power plant thermal effluent [1] and tanker oil leakage [2, 3]. Gravity currents can have a significant impact on the ecological environment of water bodies. Thermal wastewater from power plants, for example, causes serious problems in the aquatic environment [4]. In estuary areas, salt-water intrusion into freshwater degrades water quality. Gravity currents are common in lakes, estuaries [5], and oceans with a specific bed slope [6, 7]. Furthermore, gravity currents have a density interface where temperature and salinity change in discontinuities of densities, preventing material transportation in a perpendicular direction, which has an impact on the supply of nutrition [8] and oxygen [9, 10]. Before and after the gravity current passes, the material cycle around the fluid changes. Due to the climate change, the temperature between surface layer and the bottom layer increases [11], the gravity current plays an important role in the surrounding areas in ocean and lakes.

As a result, it is critical to forecast how the marine environment will change. Gravity currents has been studied extensively both experimentally and numerically. Many experiments to generate gravity currents have been carried out by opening the gate in the water tank to investigate the front speed [12, 13] and the mixture of the gravity current called lock exchange experiments.

Given the influence of the side wall of the water tank, the released fluid spreads at a constant speed at the initial stage, then slows down so that the front speed decreases with time to the power of 2/3 in the self-similar regime. When no disturbance from behind comes to the head, the current that has begun to be dominated by viscosity slows down further in the final stage dominated by viscosity, the front decelerates with the time to the power of 1/5. Each developmental stage has previously been replicated with the experiment and displayed by the box model's energy conversion [14,15]. However, the transition of the developmental stage of the gravity current without influence of the side wall of the water tank has not been clarified enough yet [16,17].

The purpose of this study is to examine how the structure of the head of gravity current changes by applying the slope limiting scheme to prevent numerical oscillation and numerical diffusion in the simulation and conducting the locked-exchange experiments. The structure of the front is very important for understanding the behavior of the front and the transport processes of materials in the vicinity.

2. RESEARCH SIGNIFICANCE

Rivers and oceans are polluted by industrial wastewater from factories and other sources as well as wastewater from everyday life, such as wastewater from household kitchens and laundry. High-density domestic wastewater flows into rivers, lakes, and other bodies of water, generating gravity currents due to different density differences and causing water pollution in these bodies of water. It is important to investigate how the leading edge of gravity current is formed and propagates in order to predict the water quality in marine and lake environments, as well as to propose new methods for controlling the effect of tsunami and other disasters.

3. METHODOLOGY

The theoretical, experimental, and numerical investigation of gravity current propagation in a long channel of length L and water depth H was conducted. Fig.1 depicts a water tank with L=4000mm length and D=60mm depth. The gate was placed from the edge of the water tank to the position of distance x_0=L/2, the fluid with the density of ρ0 was placed in one area partitioned by the gate, and the fluid with the density of ρ0+Δρ was placed in the other. As for the density difference of the fluid, the case of several percent salt water was used to do this experiment. The behavior and structure of the head of the gravity current after the gate was opened was examined.

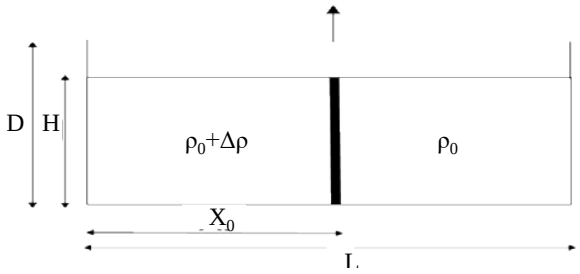

Fig.1 A schematic diagram of lock-exchange flow

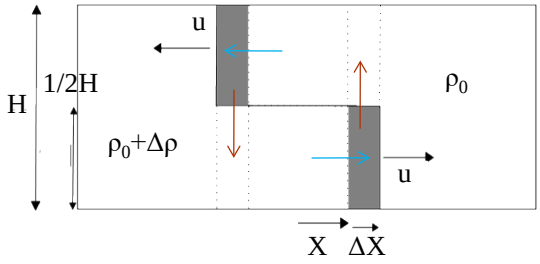

Fig.2 (a) Initial stage of gravity current

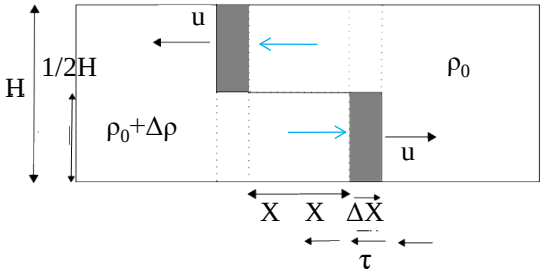

Fig.2 (b) Viscous stage of the gravity current

3.1 Boxmodel

Fig.2 (a) depicts the initial stage after the gate was opened. The fluid exchange occurred in relation to the symmetry position of the gate, the height of the gravity current became half of its initial value, and it progressed. Comparing the amount of energy change between the state after the gate was opened and the state where the head of the gravity current advanced distance x was taken into account, the amount of the change in potential energy, ΔP, by the gravity current is given by

$$\mathbf{\Delta P = -\frac{1}{4}\Delta\rho\Delta x \cdot gH^2} \quad (1)$$

where Δρ is the difference in density, Δx is the difference in distance, g is the gravitational acceleration, and H is the water depth.

It is equal to the potential energy when a heavy fluid falls only half of the initial height and is exchanged for a light fluid.

The change in kinetic energy of the head, ΔK, can be expressed as

$$\mathbf{\Delta K = \rho_0 \cdot \Delta x \cdot H \cdot v^2} \quad (2)$$

where ρ is the density of fluid in the head, and v is the characteristic velocity.

Assuming that dynamic energy is conserved and that all decreasing potential energy is used to generate kinetic energy:

$$\mathbf{\Delta P + \Delta K = 0} \quad (3)$$

therefore, the front speed is given by:

$$\mathbf{v = \frac{1}{2}\sqrt{\frac{\Delta\rho}{\rho_0} gH}} \quad (4)$$

The viscous stage is depicted in Fig.2 (b), where friction was generated between the progressing fluid and the bottom of the wall. When a rectangular area of fluid distance of x in length moved the distance of Δx along the bottom of the wall, the change in dissipa-tive energy, ΔD, can be written in the form of:

$$\Delta D = \tau x \Delta x \quad (5)$$

where shearing stress τ is regarded to be proportional to the velocity:

$$\tau = \mu \frac{1}{H} \frac{dx}{dt} \quad (6)$$

and μ denotes the viscosity coefficient of the fluid.

If the dissipative energy is entirely due to a decrease in potential energy, the moving distance x is given by:

$$x = \sqrt{\frac{1}{2}} \sqrt{\frac{\Delta\rho}{\mu} g H^3 t} \quad (7)$$

When the viscosity on the bottom wall becomes dominant, the front speed decreases as the moving distance is proportional to the time to the power of 1/2. As previously stated, gravity current progresses due to the potential energy of the density difference, and in terms of energy conversion, gravity current development stages can be divided into two stages: the initial stage and the viscous stage.

3.2 Experimental condition

An aluminum and acrylic water tank with L=4000 mm, B=100 mm in width, and D=60 mm in depth was used. The length of the water tank was long enough to investigate how the initial stage changes to the viscous stage. The tank was placed on a horizontal stand, and a partition plate that opens and closes vertically was attached. A plastic plate was used as the divider, and a guide was attached to the plate to allow it to move smoothly up and down. The gate was placed at the middle of the tank, the fluid with the density of ρ_0 was placed in one area partitioned by the gate, and the fluid with the density of $\rho_0+\Delta\rho$ was placed in the other. The less dense fluid ρ_0 was fresh water and the denser fluid $\rho_0+\Delta\rho$ was a solution of water and sodium chloride with dyed. A gravimeter and refractometer were used to measure the density ratio. The divider was opened to generate a gravity flow. A digital video camera was used to measure the position of the tip of the gravity flow. The images were captured by a computer and the elapsed time at each 50 mm distance from the gate was recorded. The water depth H was set to 25 mm, and the density differences between the two fluids are 1%, 2%, and 4%, respectively. The Reynolds numbers were 1116, 1620, and 2358, in that order.

The variables were made dimensionless by the water depth H, the propagation speed of the front $U = \sqrt{g'H}$, the advection time T=H/U, and the initial density ρ_0, where g' is the effective gravitational acceleration $g'=\Delta\rho g/\rho_0$, Reynolds number Re=UH/ν.

3.3 Numerical simulation

The Navier-Stokes equation for an inhomogeneous and incompressible fluid, the continuity equation, and the solute transport equation are the governing equations. For an accurate representation of small density difference, the density variation relative to the initial density difference was used as the primitive variable, that is, $\rho_s=(\rho-\rho_0)/\Delta\rho$, so that the non-dimensional density variations are described as $\rho_0=0.5$ for the denser fluid and $\rho_0=-0.5$ for the less density; as a result, the variation of the density is between -0.5 and 0.5.

The variables were made dimensionless by the water depth H, the propagation speed of the front $U = \sqrt{g'H}$, the advection time T=H/U, and the initial density ρ_0, where g' is the effective gravitational acceleration $g'=\Delta\rho g/\rho_0$, Reynolds number Re=UH/ν, and the diffusion parameter of density Rs=UH/κ, where ν is kinetic viscosity, and κ is the molecular diffusion coefficient of solute. $Fn=U/\sqrt{g'H}=1.0$.

The simulation conditions were matched to experimental conditions. The initial length of simulation domain was L/H=160, the grid space was $\Delta x/H=\Delta y/H=0.1$, and the time increment was set at $\Delta t/T=0.01$, the initial density difference $\Delta\rho/\rho_0=0.01$, 0.02, and 0.04. The Reynolds numbers were 1116,1620, and 2358 respectively. The non-dimensional parameter of the diffusion of solute Rs was 10^5. No-slip conditions of flow velocities were imposed at the side and bottom boundaries, and free-slip condition of flow velocities were imposed at the top of the upper boundary. In order to prevent numerical oscillation for the advective term of the transport equation of the density and the advective term of the Navier-Stokes equation, the slope limiting scheme was applied to solve the equation.

Governing equations

Transport equation for the density of the medium is described by:

$$\frac{\partial(\rho_s)}{\partial t} + \nabla \cdot (\rho_s \mathbf{u}) = Rs^{-1} \nabla^2 \rho_s \quad (8)$$

Navier-Stokes equations for viscous fluids with density change is shown by:

$$\frac{\partial(\rho \mathbf{u})}{\partial t} + \nabla \cdot (\rho \mathbf{u}\mathbf{u}) = -\nabla\varphi + Re^{-1} \nabla^2 \mathbf{u} - \rho_s F_n^{-2} \mathbf{k} \quad (9)$$

Continuity equation for incompressible fluids is expressed by:

$$\nabla \cdot \mathbf{u} = 0 \quad (10)$$

where u is the velocity vector of the medium flow, t is the time, and where is the velocity vector of the

medium flow, t is time, k is a unit vector in the vertical direction, φ is the change in pressure with respect to the hydrostatic pressure of the medium, and ρ_s is the change in density.

3.4 Application of the slope limiting scheme for 2-dimensional advection equation

The slope limiting scheme was applied to 2-dimensional advection term of the transport equation of the density and the advective term of the Navier-Stokes equation.
2-dimensional advection equation is given by:

$$\frac{\partial f}{\partial t} + c\frac{\partial f}{\partial x} + c\frac{\partial f}{\partial y} = 0 \tag{11}$$

The finite volume method is used to digitalize this equation, which is written in the form of:

$$\begin{aligned}(f_i^{n+1} - f_i^n)\Delta x + \left(F_{i+\frac{1}{2}} - F_{i-\frac{1}{2}}\right) = 0\\ \left(f_j^{n+1} - f_j^n\right)\Delta x + \left(F_{j+\frac{1}{2}} - F_{j-\frac{1}{2}}\right) = 0\end{aligned} \tag{12}$$

The value f is updated by:

$$\begin{aligned}f_i^{n+1} = f_i^n - \frac{F_{i+1/2} - F_{i-1/2}}{dx}\\ f_j^{n+1} = f_j^n - \frac{F_{j+1/2} - F_{j-1/2}}{dy}\end{aligned} \tag{13}$$

The average value of f is given by:

$$\begin{aligned}f_i^n = \frac{1}{\Delta x}\int_{x_{i-1/2}}^{x_{i+1/2}} f(x)dx\\ f_j^n = \frac{1}{\Delta y}\int_{y_{j-1/2}}^{y_{j+1/2}} f(x)dy\end{aligned} \tag{14}$$

where, function f(x), f is approximated by the straight line, which is given by:

$$\begin{aligned}f(x) = f_i + a_i(x - x_i)\\ f(y) = f_j + a_j(y - y_j)\end{aligned}$$

$$\begin{aligned}(x_i - \frac{1}{2}\Delta x < x < x_i + \frac{1}{2}\Delta x)\\ (y_j - \frac{1}{2}\Delta y < y < y_i + \frac{1}{2}\Delta y)\end{aligned} \tag{15}$$

and flux passing through cell boundaries F is shown by:

$$\begin{aligned}F_{i\pm1/2} = \int_{t^n}^{t^{n+1}} cf(t,\ x_{i\pm1/2})dt\\ F_{j\pm1/2} = \int_{t^n}^{t^{n+1}} cf(t,\ y_{j\pm1/2})dt\end{aligned} \tag{16}$$

Taking into account monotonous condition, which is given by:

$$\begin{aligned}f_{i-1}^n \geq f_i^{n+1} \geq f_i^n, f_{i-1}^n \leqq f_i^{n+1} \leqq f_i^n\\ f_{j-1}^n \geq f_j^{n+1} \geq f_j^n, f_{j-1}^n \leqq f_j^{n+1} \leqq f_j^n\end{aligned} \tag{17}$$

and the inequality concerning the slope is obtained as followed:

$$\begin{aligned}|a_i - a_{i-1}| \leq 2|a_{i-1/2}|\\ |a_j - a_{j-1}| \leq 2|a_{j-1/2}|\end{aligned} \tag{18}$$

$a_{i-1/2}$, $a_{j-1/2}$ are the slope between f [i-1], f[j-1] and f [i], f [j]. In order to satisfy the condition, the slope is limited until it is sufficient.

4. RESULT AND DISCUSSIONS

4.1 Position of the Head of Gravity Currents

In the experiment values, the distance and the time were made dimensionless by the depth H and the dimensionless time T=H/U. Fig.3 shows the position of the head of a gravity current with time, plotted with the logarithmic scale. In this case the depth was 25mm, and the density differences of two fluids were 1%, 2%, and 4%. In the case of the initial density difference 1% and 2%, the gravity current kept the constant speed, then it decelerated gradually, and decelerated with the time to the power of 1/2. When the initial density difference was 2%, the transition from the initial stage to the viscous stage was delayed behind the initial density difference of 1%. Moreover, the viscous stage was not observed for the initial density difference of 4% though the transitional period was observed. It was considered that this was because the gravity current reached the side wall before the viscous stage was observed in the water tank. At the initial stage, the gravity current advanced at the constant speed and after it decelerated gradually, it decelerated with the time to the power of 1/2 in the viscous stage. The transitional time from the initial stage to the viscous stage depends on the initial density difference and the water depth, as a result of the calculation of the transitional time with using the experimental data.

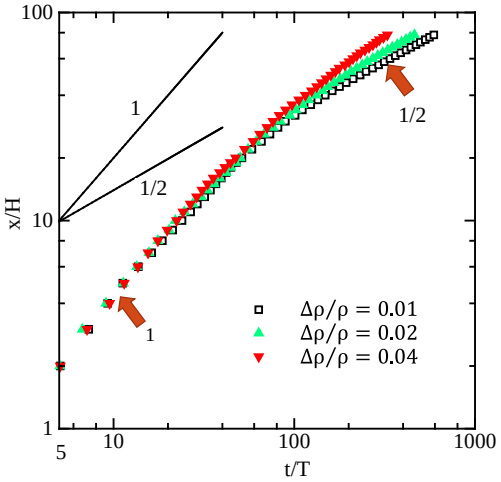

Fig.3 The position of the head of the gravity current with time in the experiment in logarithmic scale

4.2 Comparison with other TVD schemes

In order to investigate the character of slope limiting scheme that prevents numerical oscillation, the square wave and sine wave are used as the initial condition and the scheme is compared with other TVD schemes [18]- superbee, and minmod [19, 20].

4.2.1 Numerical simulation cases

The initial condition was as followed.

Case 1 square wave was used as,

$$0.0 \leq x \leq 0.15 \cdots f[x]= -1 \quad (18)$$

$$0.15 \leq x \leq 0.35 \cdots f[x]= 1 \quad (19)$$

$$0.35 \leq x \leq 0.5 \cdots f[x]= -1 \quad (20)$$

Case 2 sine wave was used as,

$$f(x)=\sin(2\pi \times x /0.5) \quad (21)$$

The calculation area was $0 \leq x \leq 0.5$, the interval of cell was 0.01, the velocity c=1.0, the interval of time dt=0.008, and the number of cells was 50.

4.2.2 The results of simulations

Fig.4 depicts a graph of the function value for square wave at t/T=10. In the case of superbee, it best preserved the shape of a square wave. Following that, the slope limiting scheme preserved the shape better than minmod. In the case of minmod, numerical diffusion occurred, and the corner just before the square was lost, resulting in the square becoming round. There was no big crumble in the shape of the wave in the case of the slope limiting scheme.

Fig.5 shows a graph of the function value at t/T=10.0 for sine wave. In the case of superbee, the curve shape of the sine wave was not preserved. When using minmod, the amplitude of the sine wave decreased, and numerical diffusion occurred. In the case of the slope limiting scheme, the shape of the sine wave was well preserved.

Given these considerations, the slope limiting scheme was appropriate for the square wave whose value changed discontinuously and the sine wave whose value changed smoothly.

In order to grasp the position of the head of the gravity current in a long channel, the slope limiting scheme that suppresses the numerical oscillations was used for solving the advection term in the transport equation for density in equation (8) and the advection term in the Navier-Stokes equation in equation (9).

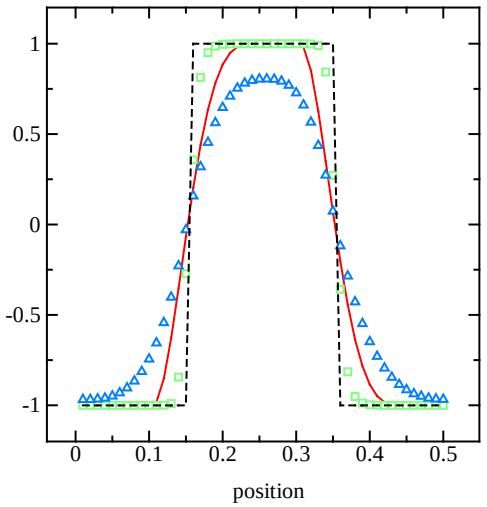

Fig.4 Numerical solutions for square wave at the non-dimensional time of t/T=10.0 Cell=50 (— slope limiting scheme, □ superbee, △ minmod, - - exact solution)

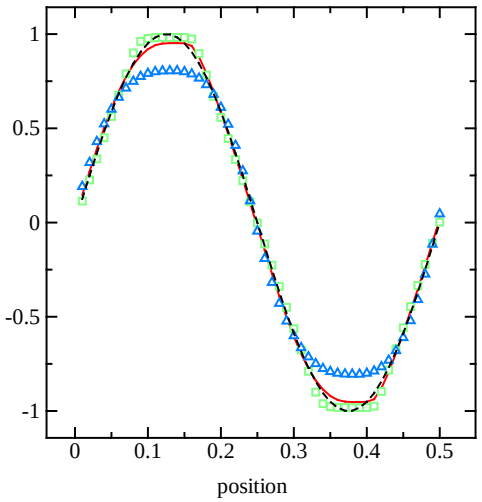

Fig.5 Numerical solutions for sine wave at the non-dimensional time of t/T=10.0 Cell=50 (— slope limiting scheme, □ superbee, △ minmod, - - exact solution)

4.3 Position of the Head of Gravity Currents

Fig.6 depicts the logarithmic relationship between the position of the head of the gravity current and the time in case of the initial density of 4% in the simulation. Because the viscous stage was not observed on the two-dimensional area of L/H=160 in the case of the initial density of 4%, it was expanded within the area of L/H=240 in the simulation.

As for the initial density difference of 1%, around time t/T=45, the initial stage changed to the transitional stage which was between the initial stage and the viscous stage just like found in the experiment. Around time t/T=125, the transitional stage changed to the viscous stage. Moreover, when

the initial density difference was 2%, around time t/T=55, the initial stage changed to the transitional stage. Around t/T=175, the transitional stage changed to the viscous stage. As for the initial density difference of 4%, around time t/T=75, the initial stage changed to the transitional stage. Around time t/T=210, the transitional stage changed to the viscous stage.

According to Fig.7, the result of the experiment and simulation were in good agreement with each other. Both the experimental and simulation results indicated that at the initial stage, the front speed advanced at a constant speed, then it slowed down, and at the final stage, dominated by the viscosity, the front decelerated with the time to the power of 1/2 when no disturbance from behind came to the head.

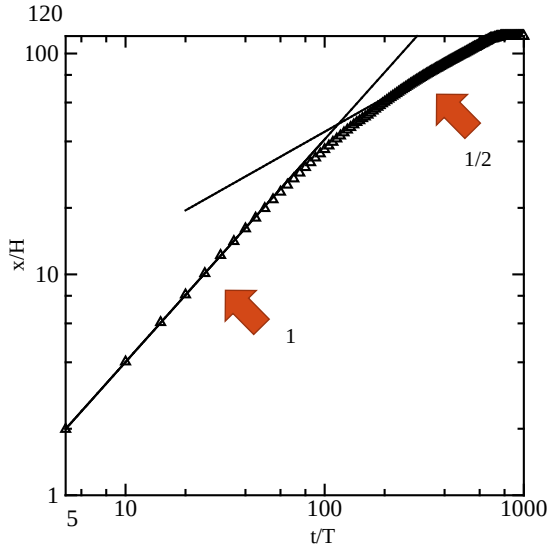

Fig.6 The position of the head of a gravity current with time in the simulation in logarithmic scale

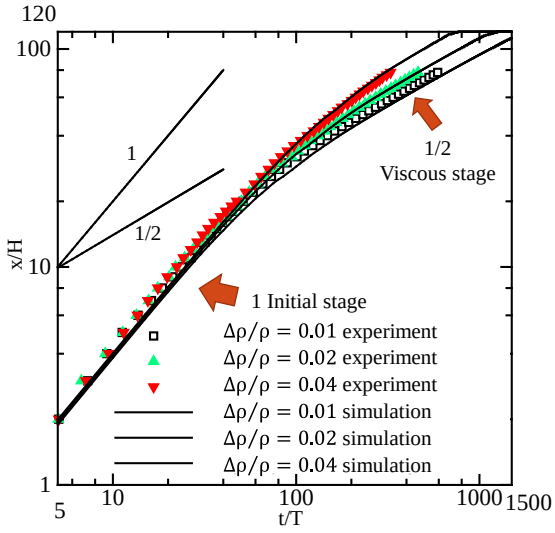

Fig.7 Comparison of the position of the head of a gravity current between experiment and simulation

4.4 Shape of the Head of Gravity Currents

The structure of the head of the gravity current propagating in a long channel was examined.

Fig.8 shows contour maps of density of gravity currents in the case of the initial density 1%, and H =25mm. The interval of the contours is 1/10 of the initial density difference. At time t/T=20, the head of the gravity current enlarged. At time t/T=80, which was between the initial stage and viscous stage, the height decreased, and the mass concentration of the head part had been reduced. The height decreased at a viscous stage, at time t/T=200, the swelling of the head had ended, and the head part had flattened. The head progressed at a constant speed when the mass was concentrated at the head. When the mass concentration at the head no longer existed, the front speed decreased with the time to the power of 1/2.

Fig.9 and 10 shows contour maps of velocity of gravity currents in the case of the initial density 1%. In the case of contour maps of vertical velocity (Fig.10), the interval of the contours is 2/100 of the initial density difference. From these contour maps, at time t/T=20 and time t/T=80, the movement in the upper fluid of the gravity current influenced the gravity current. At a viscous stage, at time t/T=200, the movement in the upper fluid did not influence the gravity current so much.

Fig.11 shows contour maps of pressure of gravity currents in the case of the initial density 1%. As the time increased, at the back of the head of gravity currents, the contour line inclined less. At a viscous stage, at time t/T=200, the contour line was horizontal. It was confirmed that there remained a strong stratified layer behind the head.

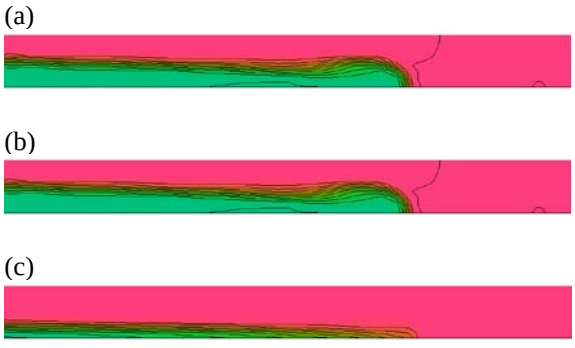

Fig.8 Contour maps of density of gravity currents at (a) t/T=20, (b) t/T=80, and (c) t/T=200 (Re=1116)

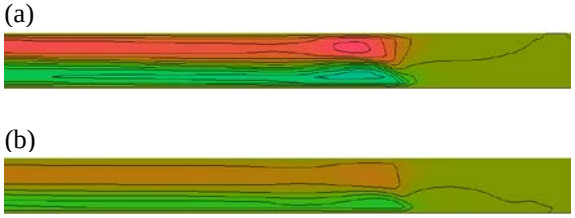

(c)

Fig.9 Contour maps of horizontal velocity of gravity currents at (a) t/T=20, (b) t/T=80, and (c) t/T=200 (Re=1116)

(a)

(b)

(c)

Fig.10 Contour maps of vertical velocity of gravity currents at (a) t/T=20, (b) t/T=80, and (c) t/T=200 (Re=1116)

(a)

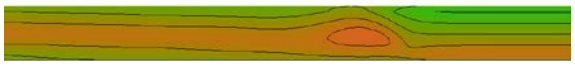

(b)

(c)

Fig.11 Contour maps of pressure of gravity currents at (a) t/T=20, (b) t/T=80, and (c) t/T=200 (Re=1116)

4.5 Time of Transition Point

The relation between the change in Reynolds number and dimensionless time of the transition point was investigated. The transition point was defined as the intersection of a straight line at the initial stage, where the front speed advanced at a constant speed, and the one at the viscous stage, where the moving distance was proportional to the time to the power of 1/2, just as shown in Fig.12. Moreover, each straight line was obtained by the least-squares method in the cases of Reynolds number 50,200,500,1116,1620,1900, and 2358.

As a result, it was found that dimensionless time of the transition point from the initial stage to the viscous stage was proportional to the Reynolds number, from the graph of Fig.13.

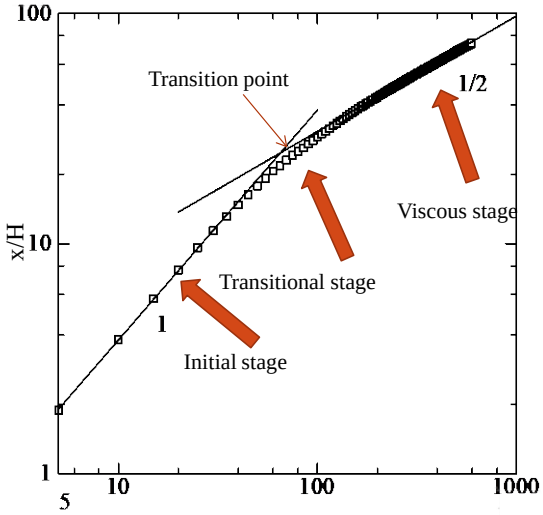

Fig.12 The position of the head of a gravity current with time in the computation in logarithmic scale (Re=1116)

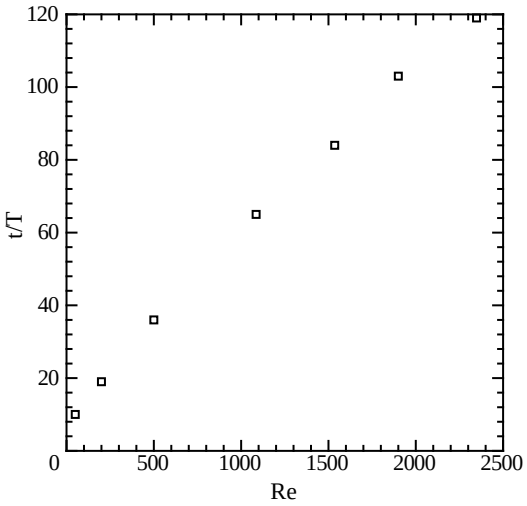

Fig.13 The time variation of the position of a gravity current in the computation showing the effect of Reynolds number

5. CONCLUSIONS

The dynamic structure of the head of the gravity current was investigated by the theory, experiment, and the simulation in the range of the Reynolds number 50-2400. The slope limiting scheme was used to prevent numerical oscillations in the density transport equation and the advective term of the Navier-Stokes equation.

The transition of the gravity current's developmental stage without the influence of the side wall of the water tank was investigated.

1. The experiment and simulation results were in good agreement with each other. The front advanced at a constant speed during the initial stage and decelerated with a time to power of 1/2 during the viscous stage.

2. At the initial stage, the gravity current caused a mass concentration at the head. The gravity current decelerated due to the influence of viscosity as the head's mass concentration decreased. At the viscous stage, mass concentration at the head was no longer present.
3. The transition from the initial stage to the viscous stage occurred at the time, which was proportional to the Reynolds number.

The engineering utility of methods to understand and alter the flow morphology of gravity flow is high. With respect to gravity flow from rivers to the ocean, a large amount of nutrients collects near the density sea surface, resulting in a large amount of phytoplankton. Predicting the head of the gravity current can contribute to fisheries that take the marine environment into account. Controlling the flow behavior of the head of the gravity current will also be useful for improving the surrounding environment, such as preventing the spread of spilled oil in the ocean and purifying the air inside buildings. In terms of disaster prevention, predicting the run-up distance of tsunamis and changing the flow pattern at the head can help prevent damage caused by tsunamis.

6. REFERENCES

[1] Simpson J.E., Gravity Currents in the Environment and the Laboratory, 2nd ed.; Cambridge University Press, 1997.

[2] Cenedese C., Nokes R. and Hyatt J., Lock-exchange gravity currents over rough bottoms, Environmental Fluid Mechanics, Vol. 18, 2018, pp. 59-73.

[3] Chai M., Yang M. and Chen Z., Analytical and numerical study of thermal and solvent-based gravity drainage for heavy oil recovery, Journal of Petroleum Science and Engineering, Vol. 208, 2022, Part B.

[4] Ho H.C. and Lin Y.T., Gravity currents over a rigid and emergent vegetated slope, Adv. Water Resour, Vol. 76, 2015, pp. 72-80.

[5] Marleau L.J., Flynn M.R. and Sutherland B.R., Gravity currents propagating up a slope in a two-layer fluid, PHYSICS OF FLUIDS, Vol. 27, 2015, 036601.

[6] Martin A., Negretti M.E., Ungarish M. and Zemach T., Propagation of a continuously supplied gravity current head down bottom slopes. Phys, PHYSICS OF FLUIDS, Vol. 5, 2020, 054804.

[7] Maggi M.R., Adduce C. and Lane-Serff G.F., Gravity currents interacting with slopes and overhangs, Advances in Water Resources, Vol. 171, 2023, 104339.

[8] Longo S., Ungarish M., Federico V. D., Chiapponi L. and Petroloa D., Gravity currents produced by lock-release: Theory and exper iments concerning the effect of a free top in non-Boussinesq systems, Advances in Water Resources, Vol. 121, 2018, pp. 456-471.

[9] Beaird N. L., Shroyer E. L., Juranek L. W., Hales B. and Goñi M. A., Nutrient-Rich Gravity Current Formed by Upwelling in Barrow Canyon; High-Resolution Observations, Journal of Geophysical Research, Vol. 125, 2020, Issue 7.

[10] Lin Y.T., Ye Y.Q., Han D.R. and Chiu Y.J., Propagation and Separation of Downslope Gravity Currents over Rigid and Emergent Vegetation Patches in Linearly Stratified Environments, Journal of Marine Science and Engineering, Vol.10, Issue 3, 2022, 308.

[11] Humphries U. and Kaewmesri P., The performance sea surface temperature anomaly over Pacific Ocean and Niño 3.4 area by using intermediate coupled model (ICM), International Journal of GEOMATE, Vol.21, Issue 84, 2022, pp. 228-235.

[12] Shin J.O., Dalziel S.B. and Linden P.F., Gravity currents produced by lock exchange, Journal of Fluid Mechanics, Vol.521, 2004, pp. 1-34.

[13] Inghilesi R., Adduce C., Lombardi V., Roman F. and Armenio V., Axisymmetric three-dimensional gravity currents generated by lock exchange, Journal of Fluid Mechanics, Vol.851, 2018, pp. 507-544.

[14] Baba N., Okamura S. and Fukuba T., Structure of head of gravity current, Journal of the society of Naval Architects of Japan, Vol. 184, 1998, pp. 197-205.

[15] Kawanaka K. and Baba N., Computation of a Gravity Current Produced by Lock Exchange Problem, Journal of the society of Naval Architects of Japan, Vol.178, 1995, pp. 119-125.

[16] Pelmard J., Norris S. and Friedrich H., Statistical characterisation of turbulence for an unsteady gravity current, Journal of Fluid Mechanics, Vol.901, 2020, Issue A7.

[17] De Falco M.C., Adduce C., Negretti M.E. and Hopfinger E.J., On the dynamics of quasi-steady gravity currents flowing up a slope, Advances in Water Resources, Vol.147, 2021, 103791.

[18] Fujii K., Numerical Calculation of Fluid Dynamics, Tokyo University Press, 1994, pp. 51-76.

[19] Baba N., Ikeda M. and Urabe E., Improvement on Computational Method For the Density Interface, Journal of the society of Naval Architects of Japan, 2007, No5K.75-76.

[20] Toro E.F., Riemann Solvers and Numerical Methods for Fluid Dynamics, A Practical Introduction, Springer-Verlag, 1999, pp. 409-474.